

Research Article

Open Access



# Intelligent data-informed study of ionospheric TEC dynamics: learning partial differential equations via PINN, PDE-Net2, and SINDy

Kening Zhang<sup>1</sup>, Zhou Chen<sup>2</sup>, Jingsong Wang<sup>3</sup>, Chuansai Zhou<sup>4</sup>

<sup>1</sup>Glasgow College, University of Electronic Science and Technology of China, Chengdu 610000, Sichuan, China.

<sup>2</sup>Institute of Space Science and Technology, Nanchang University, Nanchang 330031, Jiangxi, China.

<sup>3</sup>Key Laboratory of Space Weather, National Satellite Meteorological Center (National Center for Space Weather), China Meteorological Administration, Beijing 100081, China.

<sup>4</sup>Huawei Technologies, Shenzhen 518100, Guangdong, China.

**Correspondence to:** Prof. Zhou Chen, Institute of Space Science and Technology, Nanchang University, 999 Xuefu Avenue, Nanchang 330031, Jiangxi, China. E-mail: chenzhou@ncu.edu.cn

**How to cite this article:** Zhang, K.; Chen, Z.; Wang, J.; Zhou, C. Intelligent data-informed study of ionospheric TEC dynamics: learning partial differential equations via PINN, PDE-Net2, and SINDy. *Intell. Robot.* **2025**, 5(3), 488-504. <https://dx.doi.org/10.20517/ir.2025.25>

**Received:** 10 Feb 2025 **First Decision:** 15 Apr 2025 **Revised:** 6 May 2025 **Accepted:** 13 May 2025 **Published:** 5 Jun 2025

**Academic Editor:** Simon Yang **Copy Editor:** Pei-Yun Wang **Production Editor:** Pei-Yun Wang

## Abstract

The ionosphere is a critical region of near-Earth space, directly influencing satellite navigation and shortwave communication quality. The total electron content (TEC) is a key parameter for ionospheric physics, and AI-based research on TEC has become a major focus in space weather studies. However, current AI models often function as “black boxes” with limited physical interpretability, hindering our understanding of ionospheric dynamics. We employed two mainstream neural networks combined with partial differential equations (PDEs): PDE-Net2 (a deep learning technique capable of automatically extracting PDEs from data), physics-informed neural networks, and SINDy (a traditional method for sparse identification of PDEs), to compare the performance of these methods in reconstructing ionospheric TEC data. The comparison shows that PDE-Net2 significantly outperforms the other methods in reconstructing TEC data. Its performance metrics indicate superior effectiveness in TEC reconstruction. By directly extracting PDEs from PDE-Net2, we analyzed the expressions and found that the longitudinal convection term (e.g.,  $\frac{\partial u}{\partial x}$ ) and the latitudinal diffusion term (e.g.,  $u \cdot \frac{\partial^2 u}{\partial y^2}$ ) have the largest coefficients. This suggests that the longitudinal electron transport process in the ionosphere is the most dominant, potentially linked to the effects of longitudinal winds and diurnal solar radiation variations. Additionally, the latitudinal diffusion process plays an important role, which may involve nonlinear coupling between the Earth’s magnetosphere and ionosphere.

**Keywords:** Partial differential equation, PDE-Net2.0, PINN, SINDy, TEC



© The Author(s) 2025. **Open Access** This article is licensed under a Creative Commons Attribution 4.0 International License (<https://creativecommons.org/licenses/by/4.0/>), which permits unrestricted use, sharing, adaptation, distribution and reproduction in any medium or format, for any purpose, even commercially, as long as you give appropriate credit to the original author(s) and the source, provide a link to the Creative Commons license, and indicate if changes were made.



## 1. INTRODUCTION

The ionosphere is a critical region of space weather closely associated with human activities, with its variations directly affecting the performance of satellite navigation and radio communication systems. Currently, the total electron content (TEC) of the ionosphere is considered the most important observational parameter, as it benefits from robust data resistance to interference, global coverage of observation stations, and widespread instrument accessibility, making it the primary observational data for studying the ionospheric physical state. With the rapid accumulation of TEC data, traditional methods [International Reference Ionosphere (IRI), NeQuick] have become insufficient in capturing the complex physical variations in global TEC maps. The IRI-2016 and NeQuick2 models exhibit low prediction accuracy in sparsely observed regions, such as the Antarctic interior, where the systematic underestimation error for Slant TEC (STEC) can be as high as 30%-50%<sup>[1]</sup>. Consequently, deep learning techniques have emerged as the mainstream approach for TEC modeling and forecasting. Long short-term memory (LSTM) networks have been used to predict the spherical harmonic (SH) coefficients, enabling forecasts of global TEC maps up to 1 and 2 h ahead<sup>[2]</sup>. Similarly, the Prophet model has also been applied to predict SH coefficients, facilitating the generation of global ionospheric TEC maps with a 2-day forecasting horizon<sup>[3]</sup>. Additionally, another LSTM-based algorithm has shown excellent performance in TEC prediction, particularly due to its strong capability in capturing temporal dependencies<sup>[4-6]</sup>. In regional forecasting, LSTM models have also performed well, as demonstrated in TEC forecasting for Beijing<sup>[7]</sup>. In global forecasting, four different ConvLSTM networks have been proposed, and the multi-step auxiliary prediction (MSAP) model has been found to perform best in multi-step auxiliary forecasting tasks<sup>[8]</sup>. Further analysis has evaluated the performance of the MSAP model under varying geomagnetic storm conditions<sup>[9]</sup>. Moreover, ConvLSTM has been applied under different conditions for forecasting specific ionospheric parameters, covering a range of time spans<sup>[10,11]</sup>. A hybrid convolutional neural networks-bi-long short term memory (CNN-BiLSTM) method was used to predict ionospheric distribution during geomagnetic storm periods, with training data sourced from two solar cycles<sup>[12]</sup>. These studies demonstrate that deep learning models significantly outperform many traditional models in terms of accuracy and precision. However, these black-box models often lack interpretability in their prediction and decision-making processes.

Existing theoretical research typically explains system dynamics through partial differential equations (PDEs), such as the Navier-Stokes equations used in fluid mechanics and Newton's three laws of classical physics. Therefore, PDEs are recognized as an effective tool for explaining the nonlinear dynamic patterns of complex systems. However, relying solely on PDEs to reconstruct physical scenarios and uncover their mechanisms usually requires domain-specific knowledge and simplifications, often leading to discrepancies with actual phenomena. To more accurately learn the differential relationships from data, recent years have seen the emergence of methods combining deep learning and PDEs, which show great potential in terms of physical interpretability. In 2019, Raissi *et al.* introduced physics-informed neural networks (PINNs), integrating physical laws into the loss function, enabling neural networks to not only provide good data fitting results but also satisfy PDE constraints, thus significantly enhancing the performance and interpretability in solving both forward and inverse PDE problems<sup>[13]</sup>. In 2019, Long *et al.* proposed the PDE-Net2 method, which automatically derives PDE equations from data and has been successfully applied to the derivation of Burgers' equation, recovery of diffusion equations, and identification of convection-diffusion-reaction equations, achieving high precision<sup>[14]</sup>. In the same year, Champion *et al.* designed a deep autoencoder network combined with deep neural networks and the sparse identification of nonlinear dynamics (SINDy) model, successfully discovering control equations from scientific data<sup>[15]</sup>. In 2022, Chen *et al.* introduced a learning framework capable of automatically obtaining interpretable PDE models from sequential data, which, through extensive experiments on time series prediction in finance, engineering, and health data, validated the model's strong interpretability<sup>[16]</sup>. In 2024, Yazdani *et al.* used PINNs to optimize

the parameters of the standard k- $\epsilon$  turbulence model in fluid mechanics, demonstrating the potential of PINNs for parameter identification and optimization in fluid dynamics<sup>[17]</sup>.

In summary, research on deep learning's interpretability suggests that combining PDEs can enhance the physical interpretability of deep learning models, thereby validating and improving traditional theoretical models, uncovering the physical laws of unknown PDEs, and advancing scientific research. Current ionospheric studies mainly focus on improving prediction accuracy and observational capabilities, while research that employs deep learning to analyze ionospheric physical processes and identify the PDEs involved in these processes remains in its early stages. Therefore, this study aims to use mainstream PDE analytical methods (including both deep learning and non-deep learning approaches) to explore the dynamics of TEC. Using 2011 TEC observational data, we apply three methods - SINDy, PDE-Net2, and PINN - to conduct a physical interpretability analysis and investigate their applications in analyzing ionospheric processes. The structure of this paper is as follows: Section 2 introduces the dataset and outlines the three methods and models we evaluate; Section 3 presents results of experiment and Section 4 assesses and discusses the performance of these models.

## 2. METHODS

### 2.1. Method description

#### 2.1.1. PDE-Net 2.0

PDE-Net 2.0 is an advanced deep learning methodology designed to automatically discover PDEs from observational data. This approach combines numerical differentiation with symbolic neural networks (SymNet) to recover the PDEs that describe dynamic systems. In this framework, the input data is first processed through convolutional layers to capture spatial variations, including gradients and second-order derivatives. Subsequently, a SymNet is used to approximate the nonlinear response functions within the PDE. The code used in this study is referenced in the work of Raissi and Perdikaris<sup>[13]</sup>.

In contrast to traditional methods, PDE-Net2 does not require prior knowledge of the specific form of the PDE. Instead, it autonomously learns the various differential terms within the PDE through convolution operations on both temporal and spatial data. Compared to previous methods such as PDE-Net1.0, PDE-Net2.0 enhances the learning capability for PDE parameters by employing a numeric-symbolic hybrid deep network structure, offering greater flexibility and expressive ability. The design of the method incorporates multiple  $\delta t$ -blocks to mitigate error accumulation and improve the model's accuracy in long-term predictions, as in Figure 1. Each  $\delta t$ -block performs a prediction for a single time step, and by stacking multiple  $\delta t$ -blocks, the model can cover longer time spans, thereby enabling long-term forecasting of the system's dynamic behavior.

The optimization objective of PDE-Net2 is to minimize the prediction error at each time step while ensuring that the learned PDE satisfies the physical constraints of the data. The update formula can be given as

$$\tilde{U}(t + \delta t, \cdot) \approx \tilde{U}(t, \cdot) + \delta t \cdot \text{SymNet}_m^n(K_{00}\tilde{U}, K_{01}\tilde{U}, K_{10}\tilde{U}, \dots). \quad (1)$$

Here,  $\tilde{U}(t, \cdot)$  represents the predicted state at time  $t$ ,  $K_{ij}$  denotes the differential operators in the approximated PDE, and  $K_{ij}u \approx \frac{\partial^{i+j}u}{\partial^i x \partial^j y}$ . The  $\text{SymNet}_m^n$  is used to approximate the function  $F$ , with  $n$  depth and  $m$  variables.

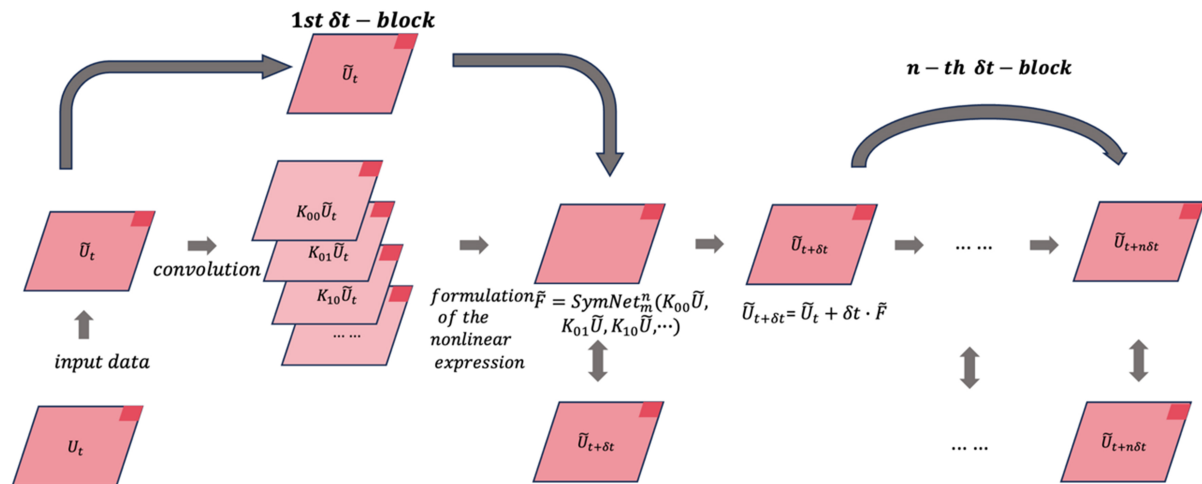


**Figure 1.** The schematic diagram of  $\delta t$ -block method.

PDE-Net2 offers significant advantages in discovering and understanding the governing equations of TEC dynamics. Specifically, it excels in several aspects: in exploring potential PDEs, this method does not require prior knowledge of the specific form of the PDE governing TEC evolution but is capable of automatically uncovering the dynamic equations of TEC changes from the data, making it particularly suitable for complex or unknown PDE problems; in enhancing interpretability, through the SymNet, PDE-Net2 can identify the components and structures of the governing PDEs that drive TEC dynamics, providing a deeper understanding of the fundamental physical processes underlying TEC variations; and in long-term prediction capability, by stacking multiple  $\delta t$ -blocks, PDE-Net2 improves its ability to reconstruct TEC dynamics over extended periods, making it more robust for practical applications.

#### 2.1.2. SINDy

SINDy is a data-driven method that discovers the simplest model describing the system's behavior through sparse regression. The first step involves constructing a feature library to represent the right-hand side (RHS) of the PDE. The feature library is generated based on observational data and its gradients, with terms including polynomial and trigonometric functions. The degree of these terms depends on the system's dynamic behavior. Next, a sparse regression method is applied to fit the model, where the feature library (RHS), time derivative data [left-hand side (LHS)], and a threshold for sparse regression coefficients are used as inputs. The regression process is solved via least squares. If a coefficient is smaller than the threshold, it is set to zero, promoting sparsity in the model. For larger coefficients, a re-application of least squares updates the coefficients. In selecting the feature library, considering that the TEC physical processes involve complex phenomena such as atmospheric motion and constitute a nonlinear system, a polynomial library is employed to capture the polynomial form of dynamic relationships. When setting the sparse regression threshold, a K-fold cross-validation procedure is utilized, which involves partitioning the dataset into several subsets, sequentially using one subset for validation while the remaining subsets are used for training. By comparing the average error of the model under different thresholds, the optimal threshold is identified, thereby effectively balancing the sparsity of the model with its predictive accuracy. The code used in this study is referenced in the work of Long et al.<sup>[14]</sup>.

The resulting sparse coefficient matrix defines the PDE for the TEC dynamical system. The sparse nature of this method ensures that the model only includes the most relevant terms, providing a concise and interpretable model. This is particularly advantageous for exploring the PDE equations governing TEC



dynamics, as it ensures the inclusion of only the most pertinent physical terms, thereby enhancing the model's interpretability and generalization ability.

### 2.1.3. PINN

PINN is a deep learning framework that combines data-driven methods with physical laws, specifically designed to solve and discover physical systems described by PDEs. The core idea of PINNs is to directly incorporate physical constraints (PDEs) into the neural network's loss function, such that the neural network learns not only from the observational data but also from the constraints imposed by the physical equations, thereby enhancing its generalization ability and physical consistency. In this study, the PDE constraints are derived using the SINDy method and are defined as  $f_u$ . The input to the network consists of spatial coordinates  $(x, y)$  and time  $t$ , with the target output being the actual observed TEC value  $u$ , and the network's predicted TEC value denoted as  $u_{pred}$ . PINN trains the neural network by minimizing a loss function, which is composed of the sum of the data fitting error and the PDE residual:

$$\mathcal{L} = \sum (u - u_{pred})^2 + \sum (f_{pred})^2 \quad (2)$$

$\sum (u - u_{pred})^2$  represents the error between the network's predicted values and the actual observed data, while  $\sum (f_{pred})^2$  indicates the degree of deviation of the predicted results from the PDE constraints. By minimizing this loss function, PINN not only fits the data but also ensures that the predictions comply with the physical laws. The training objective of PINN can be formulated as a minimization problem:

$$\min_{\theta} \mathcal{L}(\theta) = \min_{\theta} \left( \sum (u - u_{pred})^2 + \sum (f_{pred})^2 \right) \quad (3)$$

Here,  $\theta$  represents the set of parameters of the neural network. Through this optimization process, PINN gradually approaches the optimal solution, ensuring that the predictions not only match the observed data but also satisfy the physical constraints.

The training process of PINNs employs a two-stage optimization strategy: In the initial training phase, the Adam optimizer is used for global search to quickly converge to a reasonable solution space; in the fine-tuning phase, the Limited-memory Broyden-Fletcher-Goldfarb-Shanno (LBFGS) optimizer is applied for further refinement, enhancing prediction accuracy and stability. The criteria for switching optimizers are primarily twofold. First, the dynamic threshold trigger is employed: when the rate of loss decay under the Adam optimizer falls below a predefined threshold - such as when the loss change is less than  $1e-4$  for 100 consecutive iterations, the absolute loss value decreases to a certain magnitude (e.g., below  $1e-3$ ), or when the gradient norm change indicates entry into a smooth region - LBFGS is activated to accelerate local convergence. Second, a predefined phase transition is used, where the number of iterations for Adam is allocated in advance based on the problem's complexity. Once the network preliminarily captures the physical laws, it switches to LBFGS. The code used in this study is referenced in the work of Long *et al.*<sup>[14]</sup>.

## 2.2. Experiment procedure

### 2.2.1. Data selection and preprocessing

In this study, we use TEC data from the International Global Navigation Satellite System Service (IGS) center for model construction and analysis. These data are characterized by high precision and all-weather capability, making them a vital resource for ionospheric modeling. Specifically, the data used consist of 1-hour temporal resolution TEC grid data, with each TEC map having a size of  $71 \times 73$ , corresponding to approximately  $2.5^\circ \times 5^\circ$  latitude and longitude resolution, covering all latitudes and longitudes of the Earth. In these TEC maps, the value of each grid represents the vertical total electron content (vTEC) at the

corresponding location. To construct an interpretable model of the global ionosphere, we used TEC global distribution data from the entire year of 2011, consisting of 8,760 time points, and normalized the data using the min-max method. In this study, all data were used for training, with a focus on evaluating the model's reconstruction performance rather than its predictive capability. This approach in data processing helps enhance the model's performance in reconstruction tasks but may limit the assessment of its predictive ability. The coordinates of any point on Earth,  $(i, j)$ , are represented by  $(x, y)$ , where  $x$  denotes longitude and  $y$  signifies latitude, and the TEC value at that point is denoted as  $u(i, j)$ . We assume that the dynamic behavior of global TEC can be determined by a PDE.

$$\frac{\partial u}{\partial t} = f(u, \frac{\partial u}{\partial x}, \frac{\partial u}{\partial y}, \frac{\partial^2 u}{\partial x^2}, \frac{\partial^2 u}{\partial y^2}) \quad (4)$$

Here,  $f$  represents the nonlinear function governing TEC variations, and the RHS includes the TEC values and their gradients and second derivatives. After training, we validate the convergence of the loss curves for the training models (PDEnet2, PINN). By monitoring the changes in training loss, we observe whether each method progressively converges to a smaller error, thereby determining whether the model has been successfully trained.

#### 2.2.2. Evaluation

To comprehensively evaluate the performance of the three methods, both quantitative and qualitative evaluation metrics were employed.

- (1) Qualitative Analysis (Recovery TEC Maps): To qualitatively assess the fitting performance of the three methods, recovery maps were used to compare the true TEC values at time  $t_0$ , the model-reconstructed TEC values from  $t_0$  to  $t_1$ , and the true TEC values at  $t_1$ .
- (2) Qualitative Analysis (Error TEC Maps): Plot the error maps of the mean absolute error (MAE) for the reconstruction results of the three methods compared to the true values, and qualitatively analyze the performance differences among the three methods.
- (3) Quantitative Evaluation (MAE): The accuracy and stability of each method in reconstructing TEC data were quantified by calculating the MAE over 20 consecutive time steps. Lower MAE values indicate that the model's reconstructions are closer to the true values.
- (4) Quantitative Evaluation (R-square): The coefficient of determination (R-square) over 20 consecutive time steps was computed to quantify the agreement between the reconstructed TEC values and the true TEC values. The R-square value ranges from 0 to 1. A higher R-square value indicates better model performance in recovering TEC data, with a stronger correlation to the true observational data.

$$R^2 = 1 - \frac{\sum_{i=1}^n (a_i - \hat{a}_i)^2}{\sum_{i=1}^n (a_i - \bar{a})^2} \quad (5)$$

where  $a_i$  represents the actual observed values (true TEC),  $\hat{a}_i$  indicates the model's reconstructed values (reconstructed TEC values),  $\bar{a}$  is the mean of the actual observed values, and  $n$  is the total number of data points.

(5) Quantitative Evaluation [root mean square error (RMSE)]: The accuracy and stability of each method in reconstructing TEC data are quantified by calculating the RMSE over 20 consecutive time steps. Lower RMSE values indicate that the model's reconstruction is closer to the true values.

(6) *t*-test: To compare the means of PDE-Net2 with PINN and PDE-Net2 with SINDy for significant differences, an independent samples *t*-test is employed. Initially, the null hypothesis (equal sample means) and the alternative hypothesis (unequal sample means) are established. A significance level (e.g., 0.05) is selected, and the *t*-statistic is calculated along with the determination of degrees of freedom. Subsequently, the corresponding *P*-value is obtained from the *t*-distribution table or statistical software and compared to the significance level to decide whether to reject the null hypothesis. If the *t*-statistic is positive, it indicates that the mean of sample 1 is greater than the mean of sample 2. Finally, the *t*-value, degrees of freedom, *P*-value, and conclusions are reported.

$$t = \frac{\bar{X}_1 - \bar{X}_2}{\sqrt{\frac{s_1^2}{n_1} + \frac{s_2^2}{n_2}}} \quad (6)$$

$\bar{X}_1$  and  $\bar{X}_2$  are the means of the two samples,  $s_1^2$  and  $s_2^2$  are the variances of the two samples, and  $n_1$  and  $n_2$  are the sizes of the two samples.

(7) The physical meaning of the PDE terms and the physical contribution of each term were analyzed through the three methods. From the data, we extracted the PDE describing the dynamic evolution of TEC. The meanings of the terms in the PDE are as follows:

- Gradient terms  $\frac{\partial u}{\partial x}, \frac{\partial u}{\partial y}$ : These terms represent the rate of change of TEC in space, reflecting the spatial distribution of electron content in the ionosphere.
- Second-order derivative terms  $\frac{\partial^2 u}{\partial x^2}, \frac{\partial^2 u}{\partial y^2}$ : These terms describe the diffusion effects of TEC, reflecting the propagation and diffusion of plasma in the ionosphere.
- Nonlinear terms: These terms represent the nonlinear characteristics of TEC variation, which may be related to self-excited oscillations, turbulence, or other complex phenomena in the ionosphere.

Through the analysis of these terms, a deeper understanding of the physical mechanisms underlying TEC can be gained, thereby providing valuable models and reconstructive tools for ionospheric research.

### 3. RESULTS

#### 3.1. Comparison of loss curves

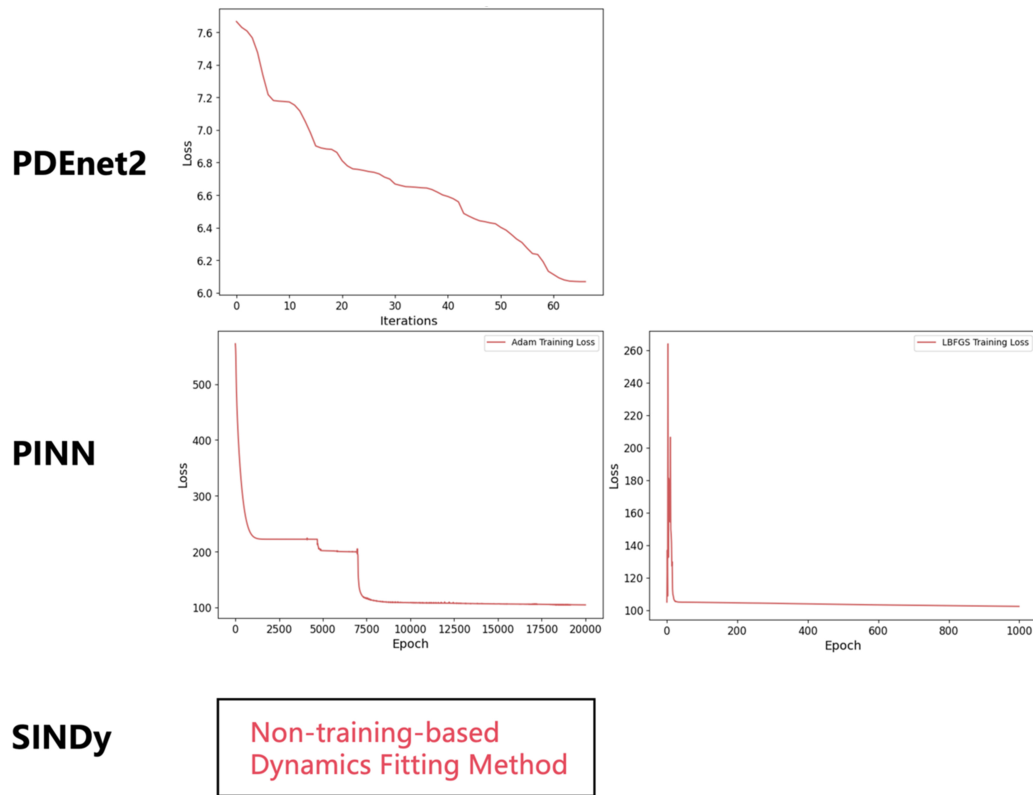
Figure 2 illustrates the learning curves of the three methods (PDEnet2, PINN, SINDy) during the training process. The loss curves for PDEnet2 and PINN exhibit a smooth decreasing trend, with the loss function gradually reducing and stabilizing as the training iterations proceed. This indicates that the training has been effectively completed, and the models are converging. The loss curve for PDEnet2 stabilizes around 6.6, while PINN converges around 100. It is noteworthy that PINN employed two different optimizers during its training process: first, the Adam optimizer for coarse optimization, followed by the LBFGS optimizer for fine-tuning, which improved the training performance and convergence speed of the model.

Table 1 presents the final loss values for both the first and second stages of the PINN method, as well as the final loss of the PDE-Net2 method. The LBFGS method provided a slight optimization based on the results from the Adam optimizer, reducing the loss by approximately 2%. The PDE-Net2 method decreased the loss from approximately 8 to around 6, demonstrating a convergent behavior.

**Table 1. Summary of the final loss values of training-based methods**

	PINN (Adam)	PINN (LBFGS)	PDE-Net2
Loss value	104.890	102.228	6.068

PINN: Physics-informed neural network; PDE: partial differential equation.



**Figure 2.** Loss curves of PDEnet2, PINN, and SINDy during training. PINN: Physics-informed neural network; SINDy: sparse identification of nonlinear dynamics.

In contrast, SINDy, as a non-training-based method, uses sparse regression to model dynamic systems, demonstrating its simplicity when handling such systems. Although SINDy does not involve a training process, it is still able to effectively capture the dynamical features of the system and automatically identify the underlying PDEs from the data. The advantage of the SINDy method lies in its rapid model derivation capability and high interpretability of the system's physical mechanisms, making it particularly suitable for scenarios where explicit physical understanding is required. However, compared to PDEnet2 and PINN, SINDy may exhibit certain limitations when dealing with complex nonlinear systems.

Overall, SINDy extracts key physical relationships from data in a more concise manner through simplified regression methods. On the other hand, PDEnet2 and PINN leverage the complexity of the data through deep learning frameworks, showcasing stronger learning capabilities and higher reconstructive accuracy, especially for modeling high-dimensional and complex dynamical systems.

### 3.2. Inference performance analysis

#### 3.2.1. Qualitative analysis

Figure 3 demonstrates the performance of the three methods in reconstructing the global TEC distribution

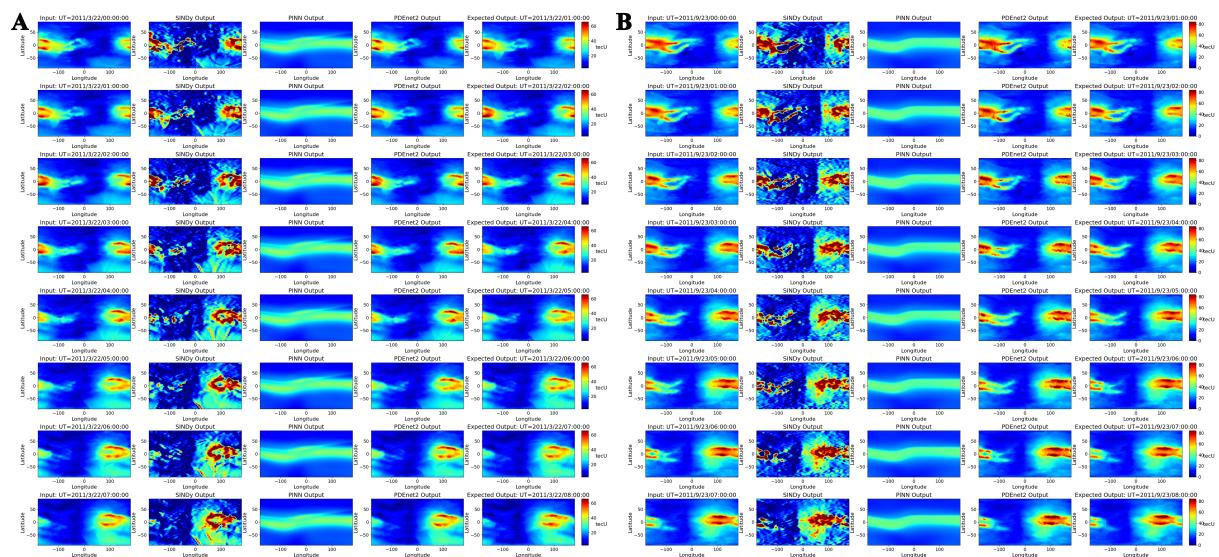


**Figure 3.** Comparison of reconstructed and true global TEC maps using PDE-Net2, PINN, and SINDy at (A) from 00:00 to 08:00 UT on March 22, 2011, (B) from 00:00 to 08:00 UT on September 23, 2011, with unit:  $\text{tecU}(10^{16} \text{ electrons/m}^3)$ . TEC: Total electron content; PDE: partial differential equation; PINN: physics-informed neural network; SINDy: sparse identification of nonlinear dynamics.

over a continuous 8-hour period during the 2011 equinoxes (from 00:00 to 08:00 UT on March 22, 2011, and from 00:00 to 08:00 UT on September 23, 2011). The figures in the leftmost column represent the input data, while those in the rightmost column stand for the true observational data used for comparison with the predicted results from the three methods. Each method reconstructed the next time step and compared the results with the true values. Specifically, the PINN method did not fully recover the true TEC distribution during reconstruction. While the reconstructed results exhibited a smooth trend, significant deviations were observed at extreme values (e.g., regions with higher TEC values), and the reconstructed TEC distribution showed some errors compared to the actual observations, indicating lower accuracy in high electron density regions. The SINDy method, although able to capture the overall trend of TEC, demonstrated a relatively coarse performance in terms of details. The reconstructed results contained substantial noise, particularly in recovering the TEC peak locations, resulting in images that lacked fine structure and high-precision reconstructions. The PDE-Net2 method performed the best in recovering the global TEC distribution. This method was able to more accurately reconstruct the peak structures of TEC, particularly in regions of the ionosphere with higher TEC values. Compared with PINN and SINDy, PDE-Net2 was more precise in capturing TEC variations, and the smoothness of the generated images and the reconstructed values were very close to the true data, yielding more accurate reconstructions.

Through a qualitative analysis of the reconstruction performance of the three methods, we found that over a period of time, the reconstruction results of PDE-Net2 are highly consistent with the real data in most regions, with its reconstructed TEC values more closely matching the trend of the original data. In contrast, PINN shows deviations in extreme value regions, failing to accurately recover the unique phenomenon of the equatorial double peaks of TEC during the equinoxes, and does not effectively capture the overall movement trend of TEC over time. Although SINDy can capture the basic trend, it exhibits lower fidelity in details, especially showing significant errors in reconstructing the positions of TEC peaks. Overall, PDE-Net2 outperforms PINN and SINDy in terms of accuracy, detailed structure, and overall trend recovery of TEC.



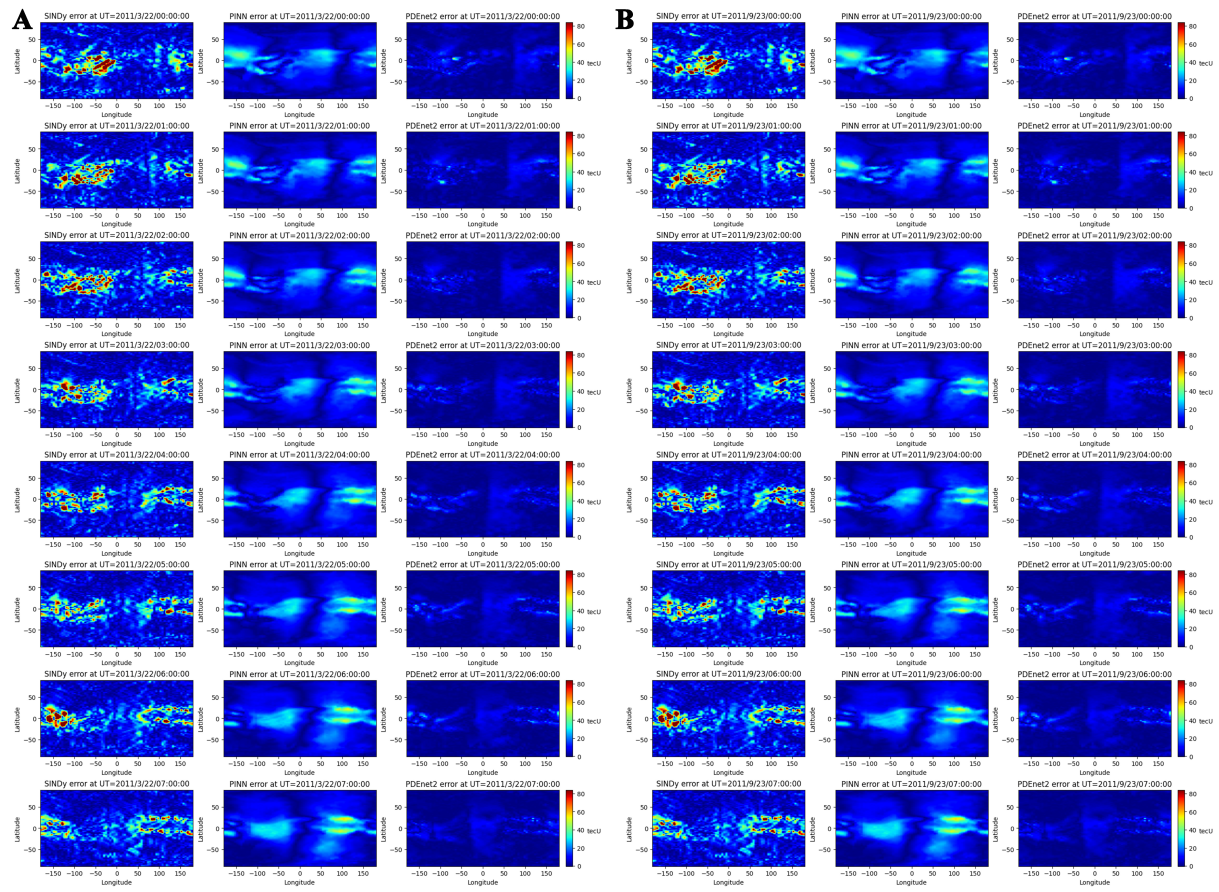


**Figure 4.** Comparison of MAE error maps of reconstructed TEC maps using PDE-Net2, PINN, and SINDy at (A) from 00:00 to 08:00 UT on March 22, 2011, (B) from 00:00 to 08:00 UT on September 23, 2011, with unit:  $\text{tecU}(10^{16} \text{ electrons/m}^3)$ . MAE: Mean absolute error; TEC: total electron content; PDE: partial differential equation; PINN: physics-informed neural network; SINDy: sparse identification of nonlinear dynamics.

Figure 4 demonstrates the MAE error map of the three methods in reconstructing the global TEC distribution over a continuous 8-hour period during the 2011 equinoxes (from 00:00 to 08:00 UT on March 22, 2011, and from 00:00 to 08:00 UT on September 23, 2011).

Through qualitative analysis of the reconstruction performance of the three methods by constructing error maps, we found that the reconstruction results of PDE-Net2 have the smallest error with the real data in most regions, showing higher data consistency. In contrast, PINN exhibits significant errors in TEC extreme value regions throughout the entire time period. While SINDy can capture basic trends, it shows significant errors in reconstructing the positions of TEC peaks at certain time points. Overall, PDE-Net2 is clearly superior to the other two methods in terms of overall accuracy and detail capture.

### 3.2.2. Quantitative analysis

Figure 5 shows the global MAE (per grid point), R-square and RMSE for the three methods PINN, PDE-Net2, SINDy at different time steps, quantifying their superiority and differences in ionospheric TEC reconstruction.



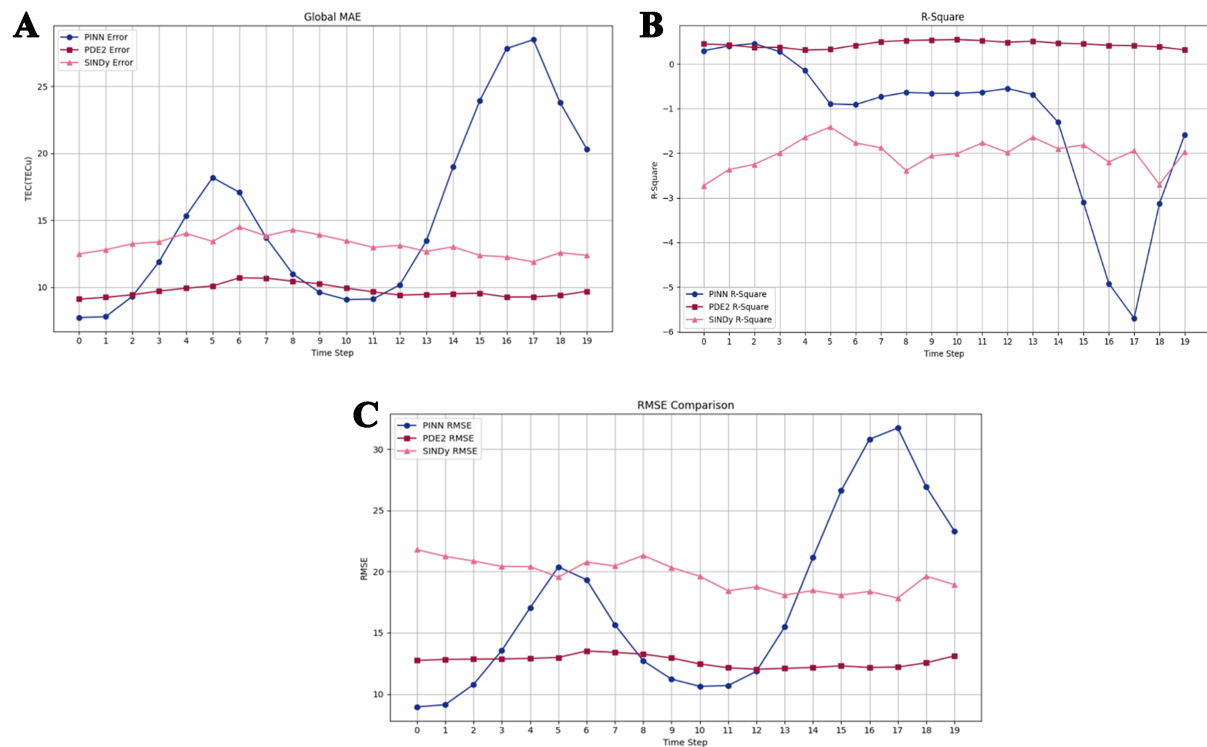


**Figure 5.** Comparison of global MAE, R-square and RMSE for PINN, PDE2, and SINDy models across different time steps. MAE: Mean absolute error; RMSE: root mean square error; PINN: physics-informed neural network; PDE: partial differential equation; SINDy: sparse identification of nonlinear dynamics.

In the global MAE analysis, the PINN method exhibits higher error values at most time steps, with a significant increase in MAE after time step 15, exceeding 25. This indicates that the model's reconstruction accuracy is relatively low during this period and fails to accurately recover the TEC data distribution. The SINDy method shows more stable performance, with an average error of around 15. In contrast, the PDE-Net2 method demonstrates lower and more stable error values at most time steps, maintaining an average error around 10. This suggests that PDE-Net2 effectively recovers the TEC distribution, exhibiting higher reconstruction accuracy and stability. In the global R-square analysis, the PINN method performed with low and highly fluctuating R-square values in most time steps, particularly at time steps 16 and 17, where the R-square value dropped below -5. The R-square values of the SINDy method were relatively stable, averaging around -2, indicating that although the method could capture the overall trend, it failed to effectively capture the details of TEC, leading to lower fitting accuracy. In contrast, the PDE-Net2 method exhibited stable R-square values around 0.6 for most time steps, demonstrating that this model could accurately fit the TEC data throughout the entire time span, exhibiting good stability.

In the global RMSE analysis, the PINN method shows higher error values for most time steps, particularly after time step 15, where the RMSE significantly increases to over 30. This indicates a marked decrease in reconstruction accuracy during these time steps, failing to effectively capture the changes in TEC data. The SINDy method demonstrates more stable performance, with RMSE values of around 20, indicating good trend capture but still leaving room for improvement in details. In contrast, the PDE-Net2 method exhibits lower and more stable RMSE values for most time steps, maintaining around 10. This suggests that PDE-Net2 has higher accuracy and consistency in reconstructing the TEC distribution.

Tables 2–4 display the  $t$ -test results for the three metrics: MAE, R-square, and RMSE. In all six comparisons, the  $P$ -values obtained are less than the significance level of 0.05, indicating that the observed results are unlikely to be due to random error, thus leading to the rejection of the null hypothesis and suggesting that the differences in sample means are significant. Based on the sign of the  $t$ -value, it can be concluded that the mean MAE of the PDE-Net2 method is significantly lower than that of the SINDy and PINN methods. Additionally, the mean R-square of the PDE-Net2 method is significantly higher than that of the SINDy and PINN methods, and the mean RMSE of the PDE-Net2 method is significantly lower than that of the SINDy and PINN methods.

From the perspective of physical interpretability, the PINN method enhances its physical constraints by embedding PDEs into the loss function. However, due to the relatively weak physical constraints, PINN fails to fully capture the detailed variations in the data when handling the complex dynamics of the ionosphere, leading to lower reconstruction accuracy and an inability to accurately recover the dynamic changes in TEC data. The SINDy method, on the other hand, directly derives the PDEs from the data through sparse regression, offering strong physical interpretability and revealing the underlying physical mechanisms of the system. However, SINDy faces certain limitations when dealing with high-dimensional, nonlinear, and complex ionospheric data, failing to fully recover the details and high peak structures of TEC, resulting in lower fitting accuracy. In contrast, the PDE-Net2 method, by combining convolutional layers with symbolic regression neural networks, not only reconstructs global TEC but also accurately reconstructs the physical processes of the complex ionosphere, effectively capturing the dynamic characteristics of the data. Therefore, the PDE-Net2 method exhibits strong accuracy and physical interpretability in ionospheric TEC modeling, providing more refined and reliable reconstruction results.

In summary, the PDE-Net2 method demonstrates clear advantages in terms of reconstruction accuracy, stability, and physical interpretability. Compared to PINN and SINDy, PDE-Net2 is better at capturing the spatiotemporal evolution of complex ionospheric data. PINN performs poorly in reconstructions at specific time steps, failing to fully capture the spatiotemporal dynamics of the ionosphere. While SINDy offers strong physical interpretability, it falls short in detail recovery and capturing high peak structures. Therefore, PDE-Net2 is the most advantageous method among the three, providing reliable support for efficient reconstruction and accurate modeling of ionospheric TEC.

### 3.2.3. Analysis of the physical significance of the PDE and the contribution of each term

Due to the suboptimal reconstruction performance of the PINN and SINDy methods, the PDE equation derived from PDEnet2 is analyzed, which is expressed as follows:

$$\begin{aligned} \frac{\partial u}{\partial t} = & 0.7 \cdot \frac{\partial u}{\partial x} + 0.24 + 0.15 \cdot u \cdot \frac{\partial u}{\partial x} + 0.11 \cdot u \cdot \frac{\partial^2 u}{\partial y^2} - 0.07 \cdot u + 0.05 \cdot \frac{\partial u}{\partial x} \cdot \frac{\partial^2 u}{\partial x \partial y} + \\ & 0.05 \cdot \frac{\partial u}{\partial x} \cdot \frac{\partial^2 u}{\partial y^2} + 0.04 \cdot \frac{\partial^2 u}{\partial x^2} + 0.04 \cdot u \cdot \frac{\partial^2 u}{\partial x^2} + 0.04 \cdot \frac{\partial^2 u}{\partial x \partial y} \cdot \frac{\partial^2 u}{\partial y^2} \end{aligned} \quad (7)$$

This PDE incorporates several mechanisms from classical physics to describe the spatiotemporal evolution of TEC. The convective term,  $0.7 \cdot \frac{\partial u}{\partial x}$ , is analogous to the convective term  $(u \cdot \nabla)u$  in the Navier-Stokes equation, reflecting the evolution of TEC along the longitude direction in space. The nonlinear convective term,  $0.15 \cdot u \cdot \frac{\partial u}{\partial x}$ , takes the same form as the nonlinear term  $u \cdot \frac{\partial u}{\partial x}$  in the Burgers equation, indicating that the TEC change rate is accelerated in regions of high electron density. The diffusion terms,  $0.04 \cdot \frac{\partial^2 u}{\partial x^2}$  and  $0.11 \cdot u \cdot \frac{\partial^2 u}{\partial y^2}$ , describe the diffusion process of TEC in space, which is similar to the diffusion term  $\nabla^2 u$  in the heat conduction equation, controlling the smoothing of TEC. The decay term,  $-0.07 \cdot u$ , is similar to the decay term  $-\lambda N$  in the radiative decay equation, describing the attenuation of TEC due to processes such as

**Table 2. t-test results for the MAE metric**

$\bar{X}_1$	$\bar{X}_2$	t value	Degrees of freedom	P value	Statistical significance
PDE-Net2	SINDy	-44.149	28	$1.298 \times 10^{-20}$	MAE (PDEnet2) < MAE (SINDy)
PDE-Net2	PINN	-3.477	28	0.002	MAE (PDEnet2) < MAE (PINN)

MAE: Mean absolute error; PDE: partial differential equation; SINDy: sparse identification of nonlinear dynamics; PINN: physics-informed neural network.

**Table 3. t-test results for the R-square metric**

$\bar{X}_1$	$\bar{X}_2$	t value	Degrees of freedom	P value	Statistical significance
PDE-Net2	SINDy	31.108	28	$9.207 \times 10^{-18}$	$R^2$ (PDEnet2) > $R^2$ (SINDy)
PDE-Net2	PINN	4.438	28	0.0002	$R^2$ (PDEnet2) > $R^2$ (PINN)

PDE: Partial differential equation; SINDy: sparse identification of nonlinear dynamics; PINN: physics-informed neural network.

**Table 4. t-test results for the RMSE metric**

$\bar{X}_1$	$\bar{X}_2$	t value	Degrees of freedom	P value	Statistical significance
PDE-Net2	SINDy	-40.488	28	$16.614 \times 10^{-20}$	RMSE (PDEnet2) < RMSE (SINDy)
PDE-Net2	PINN	-6.064	28	$7.848 \times 10^{-6}$	RMSE (PDEnet2) < RMSE (PINN)

RMSE: Root mean square error; PDE: partial differential equation; SINDy: sparse identification of nonlinear dynamics; PINN: physics-informed neural network.

electron recombination. The mixed derivative terms and higher-order cross terms reveal the complex interactions of TEC in different spatial directions, which may be related to external phenomena such as ionospheric storms and solar wind disturbances. Overall, these terms form a nonlinear reaction-convection-diffusion model, providing a physical mechanism for the dynamic evolution of ionospheric TEC.

In this equation, the magnitudes of the coefficients determine the dominance of different physical mechanisms in TEC variation as in Figure 6. The coefficient of the convective term, 0.7, indicates a strong drift tendency in the transport of TEC along the longitude direction, likely driven by longitudinal winds and diurnal solar radiation variations. In contrast, the coefficient of the nonlinear convective term, 0.15, is much smaller than that of the linear convective term, suggesting that in the complex dynamics of the ionosphere, the influence of external driving factors is greater than that of internal self-feedback mechanisms. The coefficients of the diffusion terms, 0.04 and 0.11, with the diffusion coefficient in the latitude direction (0.11) being larger, indicate that TEC propagation in the latitude direction is more significant than in the longitude direction. The TEC propagation in the latitude direction is more strongly constrained or influenced, which can be explained through the interactions between the geomagnetic field and plasma dynamics. The coefficient of the decay term, -0.07, reflects the impact of electron recombination on TEC, with the negative sign indicating that this process leads to a continual attenuation of TEC. The coefficients of the mixed derivative term, 0.05, and the higher-order cross terms, 0.04, suggest that the interactions of TEC in different spatial directions are complex but relatively weak, likely becoming significant only in cases of large local disturbances.

#### 4. DISCUSSION

In this study, we employed three methods - PDEnet2, PINN, and SINDy - to analyze and interpret the spatiotemporal evolution of the TEC in the ionosphere. Each method has its distinct advantages and limitations. In the process of solving PDEs, PDEnet2 demonstrated superior performance, particularly in

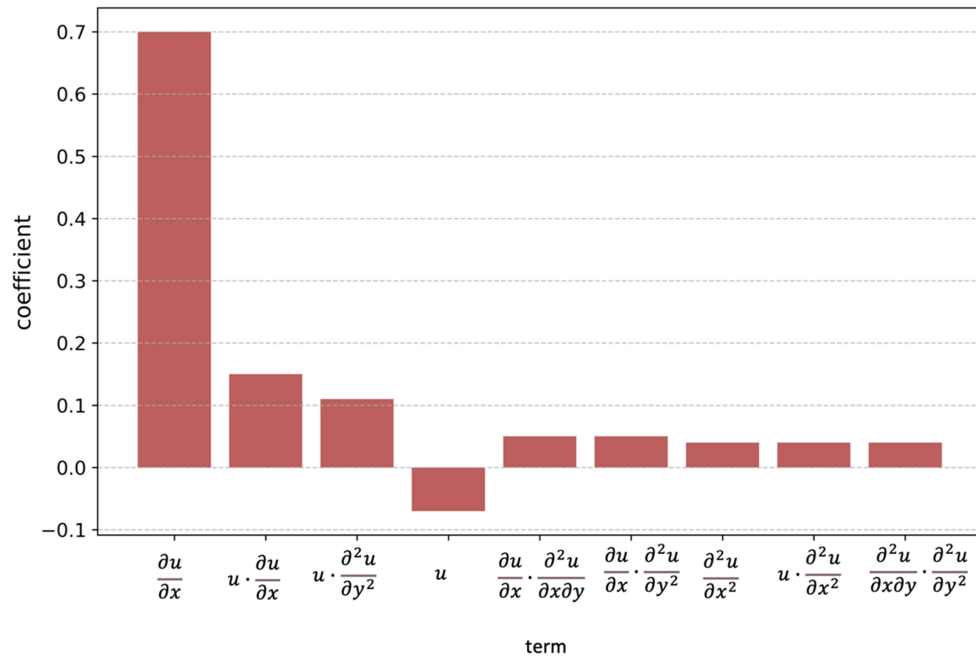


**Figure 6.** Coefficient distribution for terms in the PDE. PDE: Partial differential equation.

accurately recovering the ionospheric TEC distribution. Among the methods evaluated, PDE-Net2 demonstrates superior performance metrics compared to PINN and SINDy, establishing it as the most effective approach for TEC reconstruction. Compared to PINN, PDEnet2 more effectively captures the global structure of TEC and maintains lower errors over a larger range. Although PINN can enforce physical laws through physical constraints, its weaker constraints lead to poorer reconstruction results in extreme value regions, with significantly larger errors than PDEnet2. While SINDy can automatically derive PDEs from the data, its reconstruction results are coarser, lacking fine structures and exhibiting significant noise.

However, the use of data from a single year (2011) in this study may introduce certain limitations. As a specific phase of the solar activity cycle, the year 2011 may not fully represent the ionospheric characteristics of other years. Data from a single year might overly reflect the seasonal variations and extreme space weather events of that year, while neglecting different patterns and long-term trends that might occur in other years. Therefore, future research could consider incorporating data from multiple years to enhance the generality and robustness of the model, thereby providing a more comprehensive understanding of the dynamic behavior of the ionosphere.

In terms of the physical interpretability of ionospheric processes, PDEnet2 provides a new perspective for understanding the dynamics of the ionosphere by automatically extracting and interpreting PDEs. Further analysis of the PDE equations derived by the PDEnet2 model led to new insights into ionospheric physical processes.

Specifically, we concluded the following three points regarding the ionospheric physical processes:

(1) The longitudinal linear advection term (e.g.,  $\frac{\partial u}{\partial x}$ ) and the latitudinal diffusion term (e.g.,  $u \cdot \frac{\partial^2 u}{\partial y^2}$ ) have the largest coefficients, indicating that the electron transport process in the longitudinal direction and the diffusion process in the latitudinal direction are the most significant. From the PDE equations derived by PDE-Net2, it is evident that the changes in TEC are primarily influenced by external factors, particularly electric and wind fields. The longitudinal variation in the ionosphere is closely related to the direct influence of meridional winds in the Earth's ionosphere and the diurnal variation of solar radiation. Similarly, the latitudinal diffusion process is also crucial, potentially involving nonlinear coupling between the Earth's magnetosphere and ionosphere.

(2) The impact of the geomagnetic field on ionospheric TEC. In the PDE equation derived by PDEnet2, the diffusion coefficient in the latitude direction is relatively large (0.11), indicating that TEC propagation is more significant in the latitude direction (0.11) than in the longitude direction. The geomagnetic field in the ionosphere affects the diffusion process of TEC, particularly at different geomagnetic latitudes, where the diffusion speed and direction of plasma are influenced by the geomagnetic field. This finding suggests that TEC variations in the ionosphere are not only driven by external disturbances such as solar wind but are also constrained by changes in the geomagnetic field. During the evolution of the ionosphere, the influence of the geomagnetic field on TEC distribution cannot be ignored, especially in high-latitude regions, where TEC variations may be more strongly influenced by the magnetic field.

(3) The nonlinear feedback effects on TEC are relatively weak, primarily manifesting as enhancements in localized regions. From the nonlinear convection term,  $0.15 \cdot u \cdot \frac{\partial u}{\partial x}$  in the PDE equation derived by PDEnet2, although nonlinear feedback effects exist in regions of high electron density, these effects are relatively weak. The coefficient of this term is much smaller than that of the linear convection term (0.7), indicating that TEC variations in the ionosphere are mainly driven by external factors such as electric and wind fields, rather than by intrinsic nonlinear feedback mechanisms. Although nonlinear effects are present, their impact on TEC is relatively localized, occurring mainly in regions of higher electron density, while in other areas, the evolution of TEC is primarily controlled by external driving factors.

## 5. CONCLUSIONS

In conclusion, compared with PINN and SINDy, PDE-Net2 shows the best performance metrics, making it the most effective method for TEC reconstruction. By analyzing the PDE expressions obtained from PDE-Net2, we found three conclusions regarding ionospheric physical processes: First, the longitudinal linear convection term (e.g.,  $\frac{\partial u}{\partial x}$ ) and the latitudinal diffusion term (e.g.,  $u \cdot \frac{\partial^2 u}{\partial y^2}$ ) have the largest coefficients, indicating that the electron transport process in the longitudinal direction and the latitudinal diffusion process are the most important. Second, the geomagnetic field has a significant impact on TEC, particularly in high-latitude regions. Lastly, the nonlinear feedback effects on TEC are relatively weak, with TEC variations in the ionosphere being primarily driven by external factors. These findings provide important theoretical support for further understanding and modeling of ionospheric physical processes and offer feasible technical approaches for future ionospheric forecasting and monitoring.

## DECLARATIONS

### Acknowledgments

The implementation of the PDE-Net2 method in this study is based on the code by Long *et al.*, which can be accessed at: <https://github.com/ZichaoLong/PDE-Net/blob/PDE-Net-2.0>. The PINN part is based on the code by Raissi *et al.*, available at: <https://github.com/maziarraissi/PINNs>. The SINDy part is implemented with the code by Champion *et al.*, which can be found at: <https://github.com/kpchamp/SindyAutoencoders>. We express our gratitude to the authors of these codes for providing valuable resources that supported the

development of this research. We also appreciate the support from the China Meteorological Administration in terms of NPUs. All research results were developed based on Ascend.

### Authors' contributions

Performed experiment, data analysis and interpretation and drafted the manuscript: Zhang, K.  
Conception and design of the study, including hypothesis formulation: Chen, Z.  
Provided administrative, technical, and material support for the research design Wang, J.  
Handled data acquisition and provided technical support: Zhou, C  
All authors reviewed and approved the final manuscript.

### Availability of data and materials

The IGS TEC map data used in this study were obtained from the Space Physics Data Facility of the Goddard Space Flight Center, available online at <https://spdf.gsfc.nasa.gov/pub/data>.

### Financial support and sponsorship

This study was supported by the Key Innovation Team of “Space Weather Monitoring and Alerting” (CMA2024ZD01), the “Ionospheric Forecast and Alerting” Youth Innovation Team (CMA2024QN09), and the Jiangxi Provincial Natural Science Foundation (20224ACB211005).

### Conflicts of interest

Chen, Z. is the Guest Editor of the Special Issue of “AI for Space Information and Related Applications”. Zhou, C. is affiliated with Huawei Technologies. The other authors have declared that they have no conflicts of interest.

### Ethical approval and consent to participate

Not applicable.

### Consent for publication

Not applicable.

### Copyright

© The Author(s) 2025.

## REFERENCES

1. Jiang, H.; Liu, J.; Wang, Z.; et al. Assessment of spatial and temporal TEC variations derived from ionospheric models over the polar regions. *J. Geod.* **2019**, 93, 455–71. DOI
2. Liu, L.; Zou, S.; Yao, Y.; Wang, Z. Forecasting global ionospheric TEC using deep learning approach. *Space. Weather.* **2020**, 18, e2020SW002501. DOI
3. Tang, J.; Li, Y.; Yang, D.; Ding, M. An approach for predicting global ionospheric TEC using machine learning. *Remote. Sens.* **2022**, 14, 1585. DOI
4. Cho, K.; van, M. B.; Gulcehre, C.; et al. Learning phrase representations using RNN encoder-decoder for statistical machine translation. *arXiv* **2014**; arXiv:1406.1078. <https://doi.org/10.48550/arXiv.1406.1078>. (accessed 20 May 2025)
5. Hochreiter, S.; Schmidhuber, J. Long short-term memory. *Neural. Comput.* **1997**, 9, 1735–80. DOI
6. Yu, Y.; Si, X.; Hu, C.; Zhang, J. A review of recurrent neural networks: LSTM cells and network architectures. *Neural. Comput.* **2019**, 31, 1235–70. DOI
7. Sun, W.; Xu, L.; Huang, X.; et al. Forecasting of ionospheric vertical total electron content (TEC) using LSTM networks. In: *2017 International Conference on Machine Learning and Cybernetics (ICMLC)*, Ningbo, China. Jul 09–12, 2017. IEEE; 2017. pp. 340–4. DOI
8. Chen, Z.; Liao, W.; Li, H.; Wang, J.; Deng, X.; Hong, S. Prediction of global ionosphere TEC base on deep learning. *ESS. Open. Archive.* **2021**. DOI
9. Chen, Z.; Wang, K.; Li, H.; et al. Storm-time characteristics of ionospheric model (MSAP) based on multi-algorithm fusion. *Space.*



- Weather*. **2024**, *22*, e2022SW003360. DOI
10. Liu, L.; Morton, Y. J.; Liu, Y. ML prediction of global ionospheric TEC maps. *Space. Weather*. **2022**, *20*, e2022SW003135. DOI
  11. Xia, G.; Zhang, F.; Wang, C.; Zhou, C. ED-ConvLSTM: a novel global ionospheric total electron content medium-term forecast model. *Space. Weather*. **2022**, *20*, e2021SW002959. DOI
  12. Ren, X.; Zhao, B.; Ren, Z.; Wang, Y.; Xiong, B. Deep learning-based prediction of global ionospheric TEC during storm periods: mixed CNN-BiLSTM method. *Space. Weather*. **2024**, *22*, e2024SW003877. DOI
  13. Raissi, M.; Perdikaris, P.; Karniadakis, G. E. Physics-informed neural networks: a deep learning framework for solving forward and inverse problems involving nonlinear partial differential equations. *J. Comput. Phys.* **2019**, *378*, 686–707. DOI
  14. Long, Z.; Lu, Y.; Dong, B. PDE-Net 2.0: learning PDEs from data with a numeric-symbolic hybrid deep network. *J. Comput. Phys.* **2019**, *399*, 108925. DOI
  15. Champion, K.; Lusch, B.; Kutz, J. N.; Brunton, S. L. Data-driven discovery of coordinates and governing equations. *Proc. Natl. Acad. Sci. U. S. A.* **2019**, *116*, 22445–51. DOI
  16. Chen, Y.; Luo, Y.; Liu, Q.; Xu, H.; Zhang, D. Symbolic genetic algorithm for discovering open-form partial differential equations (SGA-PDE). *Phys. Rev. Res.* **2022**, *4*, 023174. DOI
  17. Yazdani, S.; Tahani, M. Data-driven discovery of turbulent flow equations using physics-informed neural networks. *Phys. Fluids*. **2024**, *36*, 035107. DOI